International Journal of Science Engineering and Advance Technology

Space Vector PWM Based Power Quality Compensation of Multi-Functional Grid-Tied Inverters and Its Application in Micro-Grids

[1]G.Siva Naga Malleswara Rao, [2]V.Hari Babu, [3]M.BalaSubba Reddy
[1]M.Tech, Scholar, [2]Associate Professor, [3]Associate Professor& H.O.D
Dept of EEE, Prakasam Engineering College, Kandukur.

***Abstract*— In this paper we have multi functional converters to inter connect the both the dc and ac grids to handle power quality issues of the micro-grids. Multifunctional inverters can not only interface the renewable energy resource into the utility grid, but also can compensate the harmonic and reactive current in the micro-grid as an auxiliary service. Therefore, to enhance the power quality of the micro-grid by optimal utilization of the limited and valuable capacity becomes a technical challenge. In this paper, two optimal control objectives of MFGTIs are presented based on a comprehensive power quality evaluation algorithm by means of Analytic Hierarchy Process (AHP) theory. The two proposed strategies are analyzed about the powers and voltage and currents as results, and the paper also discusses how to use them in practice for the best performance. Simulation of proposed svpwm verifies the feasibility of the proposed optimal control strategies.**

***Index Terms*— micro-grid, comprehensive power quality evaluation, Analytic Hierarchy Process, Space vector pwm, multi-functional grid-tied inverter, power quality enhancement, objective-oriented optimal control strategy.**

I. INTRODUCTION

In order to interface the stochastic and intermittent renewable energy resources (RERs) into the utility network, micro-grids are regarded as a potential solution, and these have attracted considerable attention recently [1].

Many micro-grid demonstrations integrated with RERs, energy storage devices, local loads, protective and supervisory units are described in [2-3]. Nowadays, micro-grids are a focus of research worldwide and are expected to play an important role in future electric network due to their desirable features. Firstly, micro-grids can be viewed as model citizens and/or virtual power plants to suppress the power fluctuation of RERs and make the RERs much more schedulable [4].

Secondly, the micro-grids can also improve the stability of utility and inject proper active and/or reactive power into utility in the conditions of utility failures [5]. Furthermore, because of the flexible operation modes of the micro-grids, such as grid-tied mode and islanded mode, the micro-grids can effectively enhance the operation, control, dispatch, and the black-start of utility. Finally, the micro-grids also can customize the power quality and provide flexible power supply to local loads [6].

However, the power quality requirement is always challenging the secure, stable, effective, and economic operation of micro-grids. Firstly, the parallel and/or series harmonic resonances may result in undesired trips of grid-tied inverters, and may even lead to some cascading failures [7-8]. Secondly, the harmonic and reactive current flowing across the micro-grid will cause extra power loss and lower the usage capacity of lines and loads. Particularly, the harmonic can cause vibration and noise of electric machines and transformers [9]. Finally, poor power quality will lead to poor on-grid electricity price in a power quality sensitive market in the future [10].

It is obvious that the power quality of micro-grids is a key issue for their effective and economic operation. Therefore, the power quality issue of micro-grids is drawing more and more attention. Recently, the multi-functional grid-tied inverter (MFGTI) has been

considered as a solution with high cost-effectiveness [8-10]. The so-called MFGTI is an advanced grid-tied inverter which can not only interface RERs into utility, but also enhance the power quality at its grid-tied point [4-9]. On one hand, the grid-tied inverters have the same power conversion topologies as the ones of power quality conditioners, such as active power filters (APFs), static var generators (SVGs), etc. On the other hand, in general, the capacity of a grid-tied inverter is larger than that of the installed photovoltaic arrays and/or wind turbines.

A multi-objective optimal compensation strategy is presented for 3h-bridge MFGTI application. In order to simultaneously improve power quality and satisfy the load power demand, based on the catastrophe decision theory, a quality comprehensive evaluation method is proposed in [10] to guide the optimal power quality conditioning of the MFGTI. Besides, the special 3H-bridge MFGTI in [4] is not a common used two-level converter, so the proposed optimal control is hard to be directly implemented in micro-grids or distributed generation systems. The main aim of this paper is to propose an optimal compensation strategy of MFGTIs according to the objectives based on a comprehensive power quality index (CPQI) model.

This paper is organized as follows. In Section II, the configuration and mathematical model of the micro-grid and MFGTI are introduced. Then, using the CPQI model based on Analytic Hierarchy Process (AHP) theory, the optimal compensation strategies of the MFGTI are presented in Section III where an advanced algorithm is indicated for the reference generation of the MFGTI. Implementation of Space vector pwm Is Discussed In Section IV.Simulation results with spwm are depicted in Section V to verify the feasibility of the proposed control strategy. In Section VI, simulation results with proposed control strategy of svpwm are included. Finally, conclusions are drawn in Section VII.

II. CONFIGURATION OF THE MICRO-GRID AND MATHEMATICAL MODEL OF THE MFGTI

The micro-grid demonstration as shown in Fig.1. This is a typical hybrid micro-grid including a 100kW ac sub-micro-grid and a 30kW dc sub-micro-grid.

The ac sub-micro-grid is mainly considered in this paper which consists of a 5kW permanent magnet (PM) wind generator, a 5kW direct drive PM wind power simulator, 3kW photovoltaic (PV) arrays inverters, 30kW grid-tied fuel cells, hybrid energy storage devices. Beside the fuel cell connected at bus B, other distributed generation units and local load are connected at Distribution Boxes (DB) of bus C in the test-bed room. Buses B and C are connected to 380V/50Hz three-phase three-wire distribution network by isolated transformers. The main devices of the micro-grid are listed in Table I.

TABLE I
MAIN DEVICES OF THE AC SUB-MICRO-GRID

Device	Type	Capacity	Notes
Wind generator	Source	5kW	Single-phase
PV arrays	Source	3kW	Thin-film, 1kW per phase
Diesel Generator	Source	5kW	In process
Wind power simulator	Source	5kW	Direct drive PM generator
Fuel cell	Source	30kW	Hydrogen-Oxygen
Li-ion battery	Energy storage	15kW/14.2kWh	Hybrid energy storage units
Super-capacitor	Energy storage	15kW	
MFGTIs	Source	20kW	Power quality conditioning
Controllable load	Load	30kW/15kVar	Passive loads

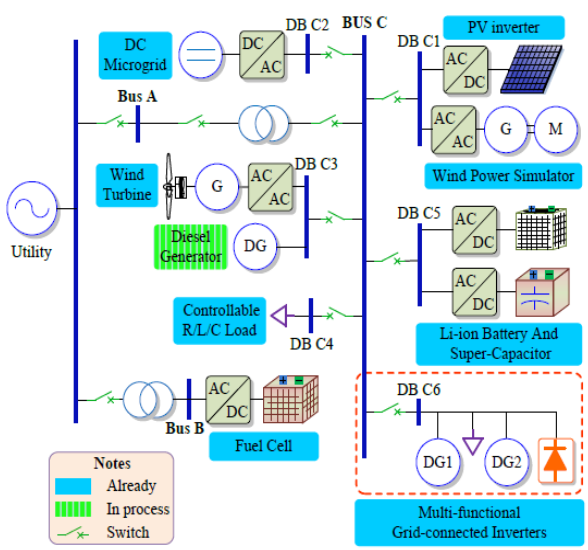

Fig.1. Configuration of the micro-grid system

From the point of view of DB C6, other feeders and the utility network can be viewed as a set of ac sources with inner inductor *Lg*, so that the feeder can be simplified as shown in Fig. 2.

Additionally, DG1 and DG2 both employ the two-level voltage source converter topology, and the detailed schematic is depicted in Fig. 3.

The dynamic response of the grid-tied current *iabc* of the MFGTI, across the filter inductor *L*, can be expressed as

$$L\dot{i}_{abc} = u_{oabc} - u_{abc} - R_s i_{abc} \quad (1)$$

where *Rs* is the parasitic resistance of the inductor, *uoabc* denotes the a.c. output voltage of the inverter, *uabc* represents the voltage at the point of inverter connection. Supposing the system is symmetrical, for arbitrary phase, the transfer functions between grid-tied current and voltage can be, respectively, expressed as

$$G_1 = I(s)/U_o(s) = 1/(Ls + R_s) \quad (2)$$

$$G_2 = I(s)/U(s) = -1/(Ls + R_s) \quad (3)$$

Furthermore, the block diagram of the grid-tied inverter can be depicted in Fig. 4.

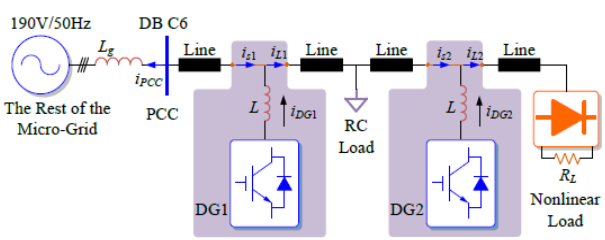

Fig 2.Single-line schematic of the feeder DBC6.

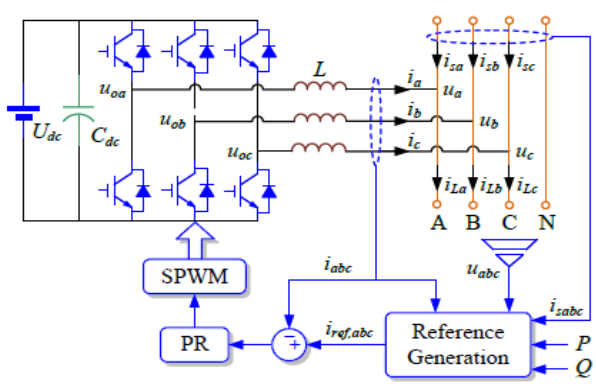

Fig.3. Topology and the overview control strategy of the MFGTI.

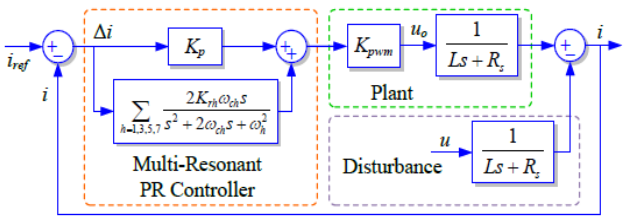

Fig.4. Control block diagram of the MFGTI.

From Fig. 3, it can be seen that each MFGTI module samples its output current *iabc* and the upstream current *isabc* flowing over it. The algorithm to calculate reference current *iref,abc* will be presented in Section III. The output current *iabc* is the feedback for tracking its reference values *iref,abc*, as shown in Fig. 4.

The multi-resonant PR controller associated with fundamental, third-, fifth-, and seventh-order harmonic components [25-27] can be expressed as

$$G_{PR}(s) = \sum_{h=1,3,5,7} \frac{2K_{rh}\omega_{ch}s}{s^2 + 2\omega_{ch}s + \omega_h^2} \quad (4)$$

where ω_1 and ω_h are the natural angular frequencies of the fundamental and h^{th}-order harmonic resonant terms, $\omega c1$ and ω_{ch} are the cut-off frequencies of these terms, K_p and K_{rh} (h = 1, 3, 5, 7) are the proportional and resonant integral gains of the PR controller.

III. OBJECTIVE-ORIENTED OPTIMAL COMPENSATION OF THE MFGTI

A. Algorithm to Generate the Reference Current:

The approaches of traditional power quality conditioners consider the harmonic and reactive current has the same weight without objective-based compensation. Unlike these conditioners, to optimally utilize the limited capacity of an MFGTI, the objective-oriented optimal compensation strategy is presented in this paper.

Besides, the harmonic and reactive current components in the micro-grid is distinguished using the different contributing weights, according to the proposed comprehensive power quality index (CPQI) model based on the Analytic Hierarchy Process (AHP) theory.

The algorithm to generate the reference current of a MFGTI is depicted in the Fig. 5. The reference current $i_{ref,abc}$ consists of two parts [11, 12, 16].

To generate the reference current, a non-phase-locked-loop (non-PLL) approach is employed to make the algorithm easy to be implemented on a DSP control board. In Fig. 5, $\theta = 2\pi ft$ is the angle corresponding to the fundamental line-frequency f of the utility network, and $T3s/2s$ represents the Clarke transformation

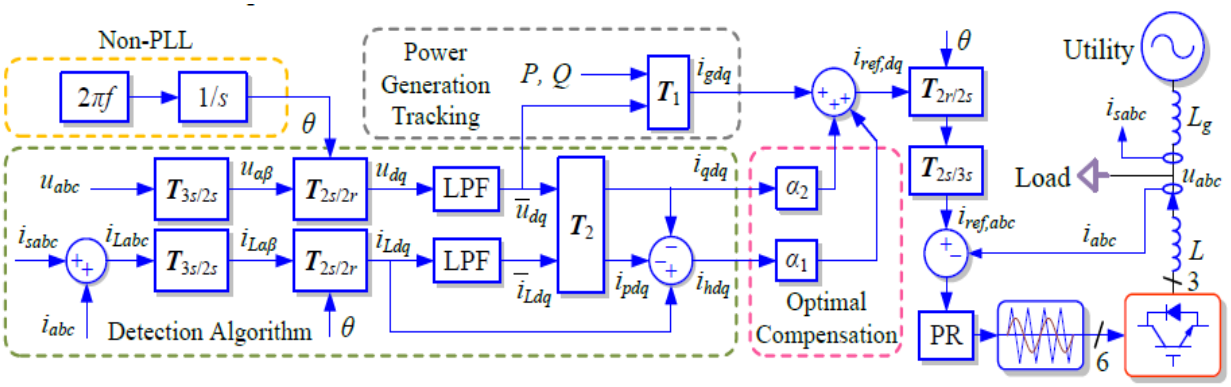

Fig.5. Algorithm for the MFGTI to Generate the Reference Current.

$$\boldsymbol{T}_{3s/2s} = \sqrt{\frac{2}{3}}\begin{bmatrix} 1 & -1/2 & -1/2 \\ 0 & -\sqrt{3}/2 & \sqrt{3}/2 \end{bmatrix} \tag{5}$$

The symbol $T_{2s/2r}$ in Fig. 5 denotes the rotating transformation

$$\boldsymbol{T}_{2s/2r} = \begin{bmatrix} \cos\theta & \sin\theta \\ -\sin\theta & \cos\theta \end{bmatrix} \tag{6}$$

for power generation in synchronous rotating dq frame, which can be expressed as

$$\begin{bmatrix} i_{gd} \\ i_{gq} \end{bmatrix} = \boldsymbol{T}_1 \begin{bmatrix} \bar{u}_d \\ \bar{u}_q \end{bmatrix} = \frac{1}{\bar{u}_d^2 + \bar{u}_q^2} \begin{bmatrix} P & Q \\ -Q & P \end{bmatrix} \begin{bmatrix} \bar{u}_d \\ \bar{u}_q \end{bmatrix} \tag{7}$$

The fundamental active and reactive components, $ipdq$ and $iqdq$, from the equivalent load current ($iLabc = isabc + iabc$) in dq frame $iLdq$, which can be written as

$$\begin{bmatrix} i_{pd} \\ i_{pq} \end{bmatrix} = \frac{\bar{u}_d \bar{i}_{Ld} + \bar{u}_q \bar{i}_{Lq}}{\bar{u}_d^2 + \bar{u}_q^2} \begin{bmatrix} 1 & 0 \\ 0 & 1 \end{bmatrix} \begin{bmatrix} \bar{u}_d \\ \bar{u}_q \end{bmatrix} \tag{8}$$

$$\begin{bmatrix} i_{qd} \\ i_{qq} \end{bmatrix} = \frac{\bar{u}_q \bar{i}_{Ld} - \bar{u}_d \bar{i}_{Lq}}{\bar{u}_d^2 + \bar{u}_q^2} \begin{bmatrix} 0 & 1 \\ -1 & 0 \end{bmatrix} \begin{bmatrix} \bar{u}_d \\ \bar{u}_q \end{bmatrix} \tag{9}$$

Then, the harmonic current in dq frame can be expressed as

$$i_{hdq} = i_{Ldq} - i_{pdq} - i_{qdq} \tag{10}$$

In summary, the detected harmonic and reactive equivalent load current in dq frame is multiplied by the optimal compensation coefficients, namely $\alpha 1$ and $\alpha 2$, and added to the reference current for power generation $igdq$ to form the reference current in dq frame. With the help of the inverse transformations, the reference current in abc frame can be derived. The optimal compensation coefficients can be obtained in the following subsection.

B. Model and Solution of the Objective-Oriented Optimal Compensation Strategy

The CPQI model to evaluate the power quality at PCC of the micro-grid can be depicted in Fig. 6 using the AHP theory. According to the AHP-based CPQI model, the total harmonic distortion (THD) and power factor (PF) of the current flowing across the PCC contribute the CPQI F with different weights $\omega 1$ and $\omega 2$.

The comparison matrix can be chosen as

$$\boldsymbol{C} = \begin{bmatrix} 1 & 3 \\ 1/3 & 1 \end{bmatrix} \tag{11}$$

The eigenvalues and eigenvectors of C can be derived, and the coincident justice can be written as

$$CI = (\lambda_{\max} - n)/(n-1) \tag{12}$$

Where $\lambda \max = 2$ is the maximum eigen value of C, and $n = 2$ is the order of C. It can be found that $CI = 0$, so the

coincident judgment is passed according to the AHP theory. Normalized the eigenvector corresponding to the maximum eigen value λmax, the weights of the CPQI model can be obtained as ω = (ω1, ω2) = (0.75, 0.25).

According to the CPQI model in Fig. 6, the CPQI can be expressed as $F = \omega 1\gamma h + \omega 2\gamma q$, where γh and γq are the harmonic and reactive coefficients of PCC current will be defined in the following part.

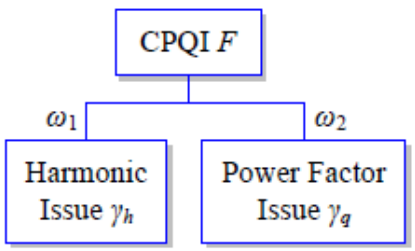

Fig.6. Model of comprehensive power quality evaluation

.

In the following parts, two different objectives are proposed based on the aforementioned CPQI model for the optimal compensation of the MFGTI.

1) Objective I: Employing minimum capacity to maximally enhance the power quality of the micro-grid

1. Objective function: In such objective, the capacity of the MFGTI employed for power quality compensation can be expressed as

$$S = \sqrt{S_h^2 + S_q^2} = 3U\sqrt{(\alpha_1 I_{h0})^2 + (\alpha_2 I_{q0})^2} \qquad (13)$$

where *Sh* and *Sq* are the capacity of the MFGTI employed for harmonic and reactive compensation, respectively, *U* is the root-mean-square (RMS) value of the utility phase-to-ground voltage, *Ih*0 and *Iq*0 are the RMS values of the harmonic and reactive current before the MFGTI starts to compensate, α1 and α2 are the optimal compensation coefficients of the MFGTI for power quality enhancement. Therefore, the optimal compensation objective I can be chosen as

$$\min\ F_1 = S^2/(9U^2) = \alpha_1^2 I_{h0}^2 + \alpha_2^2 I_{q0}^2 \qquad (14)$$

Where

$$\begin{cases} I_{h0} = \gamma_{h0} I_1 \\ I_{q0} = \gamma_{q0} I_1 \end{cases} \qquad (15)$$

where γh0 and γq0 are the initial harmonic and reactive coefficients of PCC current *iPCC* before the compensation of the MFGTI, respectively. γh0 can be chosen as the THD, while γq0 is defined as the ratio between reactive and fundamental components of the current, even as the RMS value ratio between the reactive current *Iq* and fundamental current *I*1, which can be expressed as

$$\gamma_q = Q/(3UI_1) = (3UI_q)/(3UI_1) = I_q/I_1 \qquad (16)$$

2. Supposing the harmonic and reactive coefficients of the PCC current are γh and γq after the compensation of the MFGTI, the CPQI in such a condition can be written as

$$\omega_1\gamma_h + \omega_2\gamma_q = A \qquad (17)$$

where *A* is the set target and is a constant. The target CPQI *A* of the micro-grid at PCC should be set according to the power quality standards of the utility or the schedule of the utility. On one hand, according to the power quality regulations in the utility, the THD and PF should be controlled in the proper ranges, such as THD < 5% and PF > 0.98.

Therefore, the target *A* can be directly calculated according to the power quality regulations in such conditions. On the other hand, as indicated in [29], the grid-tied inverters should be scheduled to participate in many services of the utility, such as reactive power supporting, power quality enhancement, and so on. In such conditions, to support the power quality enhancement and reactive stability of the utility, the CPQI *A* can be given by the distribution network operator and guides the MFGTI to generate the desired harmonic and reactive power into utility. It should be noted that a smaller *A* represents better power quality level of the micro-grid. Therefore, the set CPQI *A* should be smaller than the one σ before the compensation of the MFGTI which can be expressed as

$$\sigma = \omega_1\gamma_{h0} + \omega_2\gamma_{q0} \qquad (18)$$

Apparently, if all the harmonic and reactive current components are compensated, γh and γq should be zeroes, so that CPQI $F = A = 0$.

Generally, the load power demand and the power generation of DGs are constant in a time interval,

the RMS value of the fundamental current is approximately the same before and after compensation of the MFGTI. For convenience, $I1$ is considered as constant. In ideal conditions, the harmonic and reactive coefficients, after the compensation of the MFGTI, can be expressed as

$$\begin{cases} \gamma_h = (1-\alpha_1)\gamma_{h0} \\ \gamma_q = (1-\alpha_2)\gamma_{q0} \end{cases} \quad (19)$$

Where $\alpha1$ and $\alpha2$ are the ratios of compensated harmonic and reactive current components in the micro-grid. Thus, the remaining harmonic and reactive coefficients after the MFGTI starts to compensate should be $(1 - \alpha1)$ and $(1 - \alpha2)$ of the initial ones, respectively.

3. Lagrange's function to solve the objective model can be written as

$$L_1 = \alpha_1^2 I_{h0}^2 + \alpha_2^2 I_{q0}^2 + \lambda_1(\omega_1\gamma_h + \omega_2\gamma_q - A) \quad (20)$$

Where $\lambda1$ is the Lagrange multiplier of objective I, in unit $I2$/CPQI. It should be noted that, if no power quality compensation action is taken, the Lagrange's function meets $L1 = 0$ in the condition of $\alpha1 = \alpha2 = 0$ and $A = \sigma$.

On the contrary, if all the harmonic and reactive current is compensated, $L1$ is in the condition of $\alpha1 = \alpha2 = 1$ and $A = 0$. Thus, the value of Lagrange's function $L1$ is within the interval $[0, I^2_{ho}+I^2_{F0,}]$. According to (20), it can be found that

$$\begin{cases} \partial L_1/\partial\alpha_1 = 2\alpha_1(\gamma_{h0}I_1)^2 - \lambda_1\gamma_{h0}\omega_1 = 0 \\ \partial L_1/\partial\alpha_2 = 2\alpha_2(\gamma_{q0}I_1)^2 - \lambda_1\gamma_{q0}\omega_2 = 0 \\ \partial L_1/\partial\lambda_1 = \omega_1\gamma_h + \omega_2\gamma_q - A = 0 \end{cases} \quad (21)$$

Therefore, the solutions of the optimal model can be written as

$$\begin{cases} \alpha_1 = (\sigma - A)\omega_1/\left[(\omega_1^2+\omega_2^2)\gamma_{h0}\right] \\ \alpha_2 = (\sigma - A)\omega_2/\left[(\omega_1^2+\omega_2^2)\gamma_{q0}\right] \\ \lambda_1 = 2(\sigma - A)I_1^2/(\omega_1^2+\omega_2^2) \end{cases} \quad (22)$$

It can be seen that the optimal compensation coefficients $\alpha1$ and $\alpha2$ are related to the weights $\omega1$ and $\omega2$, so the approaches to get the CPQI may affect the optimal compensation strategy. Thus, except for AHP approach, some other power quality comprehensive evaluation approaches can be employed for the objective-oriented compensation of MFGTI and may get some different results [24].

According to the analysis mentioned before, flowchart to obtain the optimal compensation coefficients of the objective I model can be demonstrated in Fig. 7(a). It should be noted that, by means of energy management system (EMS), this optimal calculation can be completed in the tertiary control of a hierarchical controlled micro-grid [30]. Then, according to the dynamic generation and load levels, the EMS downloads the optimal coefficients $\alpha1$ and $\alpha2$ to the MFGTI controller in real time.

In Fig. 7(a), as aforementioned, the parameters $\gamma h0$ and $\gamma q0$ are the harmonic and reactive coefficients of PCC current, respectively, before the MFGTI compensates the power quality issues. Additionally, parameters $\omega1$ and $\omega2$ are weights of the power quality indicators and can be set by the mentioned AHP-based CPQI model. Thus, σ is the CPQI in the condition of $\gamma h0$, $\gamma q0$, $\omega1$, and $\omega2$, as shown in (18). For any given CPQI A, it can be found an optimal solution ($\alpha1$, $\alpha2$) according to the flowchart in Fig. 7(a).

When the given CPQI A varies in the interval $[0, \sigma]$, the solution set of optimal compensation coefficients for objective I application can be obtained. It should be noted that when the compensation coefficient of one power quality indictor larger than 1, this power quality indictor can be considered to be eliminated in the AHP-based CPQI model.

Then, the algorithm repeats the calculation in (20)-(22) and calculates the compensation coefficient of the left power quality indictor.

2) Objective II: Minimizing the CPQI in the condition of given capacity for power quality enhancement

According to the comprehensive power quality evaluation model, the optimal objective II can be expressed as

$$\min \ F_2 = \omega_1\gamma_h + \omega_2\gamma_q \quad (23)$$

1. Supposing the given capacity of the MFGTI for power quality enhancement is set as Sg, it can be written as

$$S_g = 3U\sqrt{\alpha_1^2 I_{h0}^2 + \alpha_2^2 I_{q0}^2} \quad (24)$$

2. According to (23) and (24), the Lagrange's function can be chosen as

$$L_2 = \omega_1\gamma_h + \omega_2\gamma_q + \lambda_2\left(3U\sqrt{\alpha_1^2 I_{h0}^2 + \alpha_2^2 I_{q0}^2} - S_g\right) \quad (25)$$

where Sg is the available margin capacity of the MFGTI, λ2 is the Lagrange multiplier of objective II, in unit CPQI/S.

According to (25), it can be derived that

$$\begin{cases} \partial L_2/\partial\alpha_1 = -\omega_1\gamma_{h0} + 3\lambda_2 U\alpha_1 I_{h0}^2 \Big/ \sqrt{\alpha_1^2 I_{h0}^2 + \alpha_2^2 I_{q0}^2} = 0 \\ \partial L_2/\partial\alpha_2 = -\omega_2\gamma_{q0} + 3\lambda_2 U\alpha_2 I_{q0}^2 \Big/ \sqrt{\alpha_1^2 I_{h0}^2 + \alpha_2^2 I_{q0}^2} = 0 \\ \partial L_2/\partial\lambda_2 = \alpha_1^2 I_{h0}^2 + \alpha_2^2 I_{q0}^2 - S_g^2/(9U^2) = 0 \end{cases} \quad (26)$$

Then,

$$\begin{cases} \alpha_1 = \omega_1\gamma_{h0} S_g I_{q0} \Big/ \left(3UI_{h0}\sqrt{(\omega_1\gamma_{h0}I_{q0})^2 + (\omega_2\gamma_{q0}I_{h0})^2}\right) \\ \alpha_2 = \omega_2\gamma_{q0} S_g I_{h0} \Big/ \left(3UI_{q0}\sqrt{(\omega_1\gamma_{h0}I_{q0})^2 + (\omega_2\gamma_{q0}I_{h0})^2}\right) \\ \lambda_2 = \sqrt{(\omega_1\gamma_{h0}I_{q0})^2 + (\omega_2\gamma_{q0}I_{h0})^2} \Big/ (3UI_{h0}I_{q0}) \end{cases} \quad (27)$$

Unlike the situations mentioned before in the part about objective I, when the optimal compensation coefficient of one power quality indictor approaches 1, the calculation for another indictor should be paid special attention, and the model in (23)-(27) should be rebuilt. For instance, if the optimal coefficient of harmonic component $\alpha 1$ reaches at 1 firstly, the coefficients $\alpha 2$ and $\lambda 2$ should be calculated as

$$\begin{cases} \alpha_2 = \sqrt{S_g^2 - (3UI_1\gamma_{h0})^2} \Big/ (3UI_1\gamma_{q0}) \\ \lambda_2 = \sqrt{\alpha_2^2(\gamma_{q0}I_1)^2 + (\gamma_{h0}I_1)^2} \Big/ (3U\alpha_2\gamma_{q0}I_1^2) \end{cases} \quad (28)$$

According to (27) and (28), the flowchart to obtain the optimal compensation coefficient can be depicted in Fig. 7(b). It can be seen that, for any given *Sg* in the interval [0, *S*0], the proposed model can achieve an optimal solution ($\alpha 1$, $\alpha 2$) for objective II application.

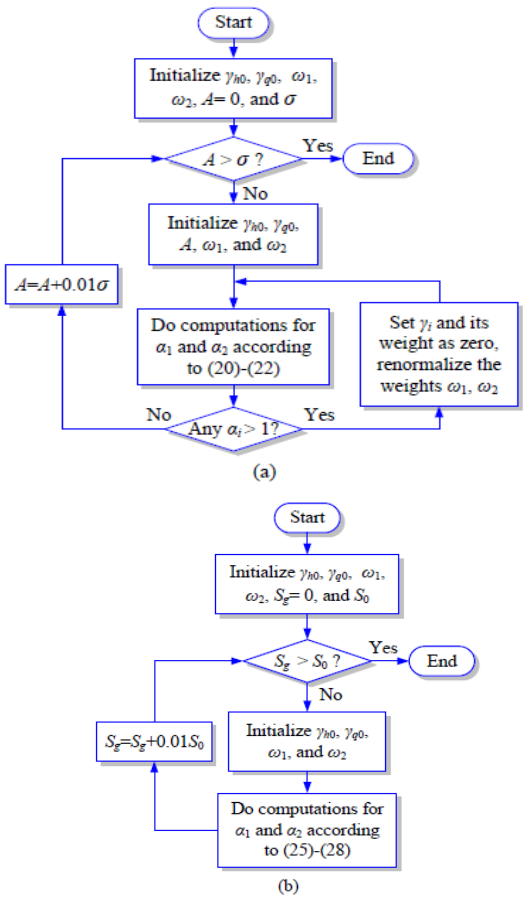

Fig. 7. Flowcharts to solve the optimal compensation model of the MFGTI according to (a) objective I for $A \in [0, \sigma]$ and (b) objective II for $S_g \in [0, S_0]$.

According to (27) and (28), the flowchart to obtain the optimal compensation coefficient can be depicted in Fig. 7(b). It can be seen that, for any given *Sg* in the interval [0, *S*0], the proposed model can achieve an optimal solution ($\alpha 1$, $\alpha 2$) for objective II application.

IV. IMPLEMENTATION SPACE VECTOR PULSE WIDTH MODULATION

SVPWM aims to generate a voltage vector that is close to the reference circle through the various switching modes of inverter. Figure 3 is the typical diagram of a three-phase voltage source inverter model. S1 to S6 are the six power switches that shape the output, which are controlled by the switching variables a, a‟, b, b‟, c and c‟. When an upper transistor is switched ON, i.e., when a, b or c is 1, the corresponding lower transistor is switched OFF, i.e., the corresponding a‟, b‟ or c‟ is 0. Therefore, the ON and OFF states of

the upper transistors S1, S3 and S5 can be used to determine the output voltage. Hence there are 8 possible switch states, i.e.,(0,0,0), (0,0,1), (0,1,0), (0,1,1), (1,0,0), (1,0,1), (1,1,0), (1,1,1).

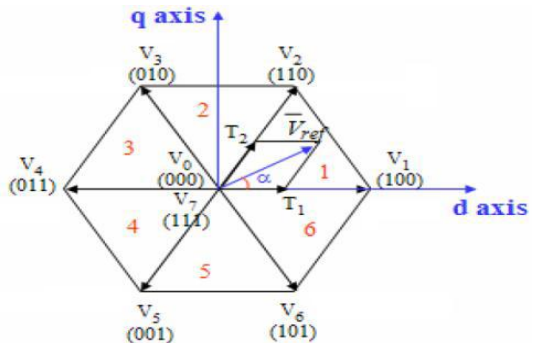

Fig.8: Basic switching vectors and sectors

TABLE II

Switching vectors, phase voltages and output line to line voltages

Voltage Vectors	Switching Vectors			Line to neutral voltage			Line to line voltage		
	a	b	c	V_{an}	V_{bn}	V_{cn}	V_{ab}	V_{bc}	V_{ca}
V_0	0	0	0	0	0	0	0	0	0
V_1	1	0	0	2/3	-1/3	-1/3	1	0	-1
V_2	1	1	0	1/3	1/3	-2/3	0	1	-1
V_3	0	1	0	-1/3	2/3	-1/3	-1	1	0
V_4	0	1	1	-2/3	1/3	1/3	-1	0	1
V_5	0	0	1	-1/3	-1/3	2/3	0	-1	1
V_6	1	0	1	1/3	-2/3	1/3	1	-1	0
V_7	1	1	1	0	0	0	0	0	0

V.SIMULATION RESULS WITH SPWM CONTROLLER

TABLE III

IMPORTANT PARAMETERS OF THE MFGTI PROTOTYPE

U_{dc} (V)	L (mH)	R_s (Ω)	C_{dc} (μF)	R_L (Ω)	L_g (mH)
350	0.5	0.05	4400	20	3

A. Performance of MFGTI on Power Generation with Spwm

To verify the performance of the designed ulti-resonant PR controller on current-tracking for power Generation of RERs, the steady-state and dynamic responses of the MFGTI have been checked, in the condition of that its reference active and reactive power steps from 4kW to 6kW, and from 2kVar to – 2kVar respectively. .

Fig. 17 depicts the steady-state performance of the MFGTI on the PF, THD, and the efficiency. It can be seen that when the reference active power is larger than 3kW, the THD will drop below 5%. Due to the zero-phase-shift feature of the multi-resonant PR controller, the PF of the grid-tied current of the MFGTI can be maintained at a very high level. Additionally, the efficiency of the MFGTI will increase when the reference active power increases

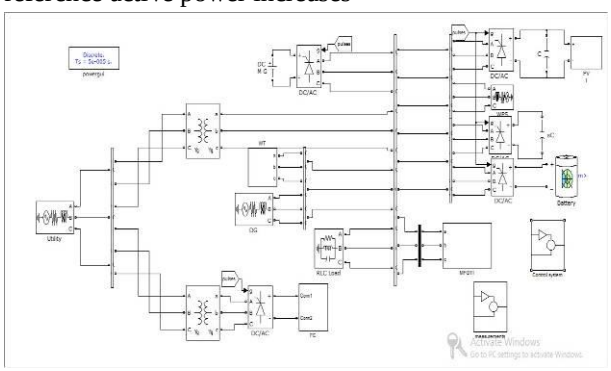

Fig.9. Simulink Model of MFGTI

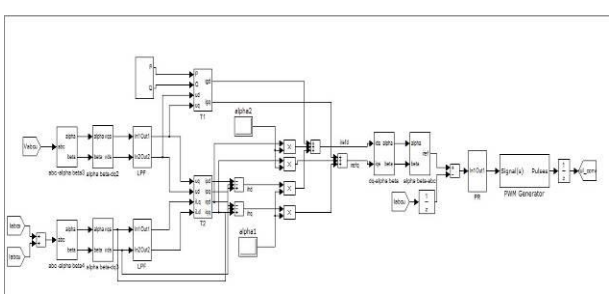

Fig.10. svpwm controller for generation of gate pulses

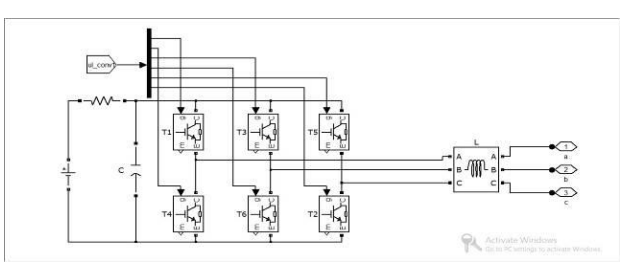

Fig.11. dc link connected inverter

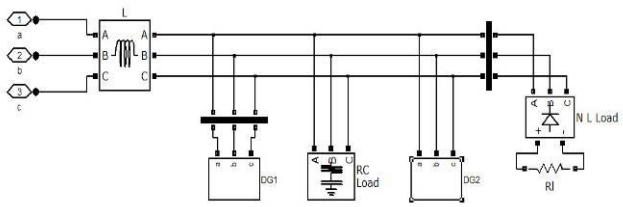

Fig .12.. Inter Connection Of Distributed Generations DG1 & DG2

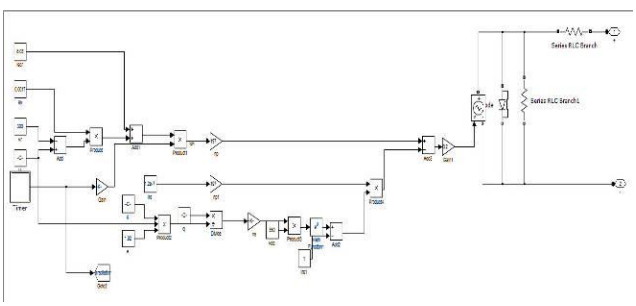

Fig .13 simulink model of pv panel module

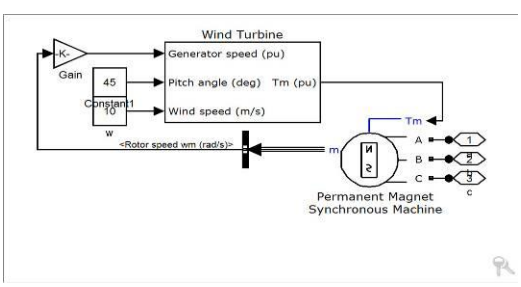

Fig.14. simulink model of wind turbine

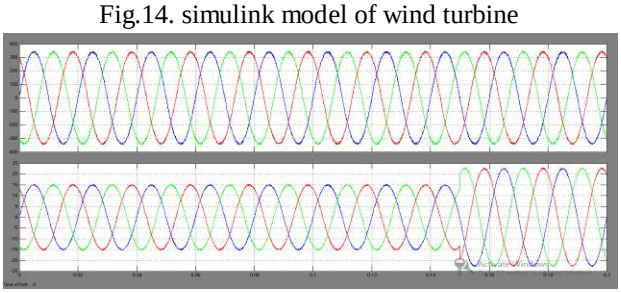

Fig.15. Three Phase Output Voltges(Vabc) And Currents(Iabc)

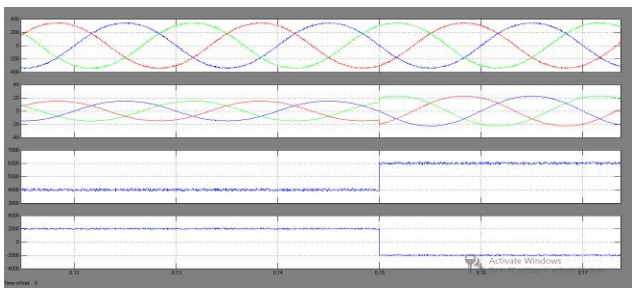

(a)

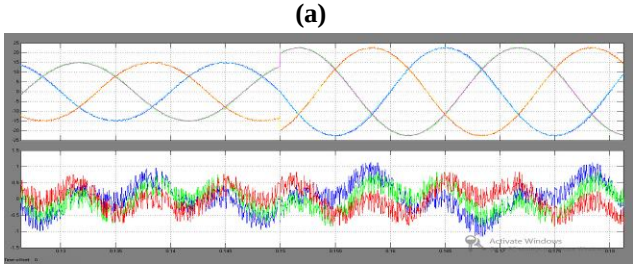

(b)

Fig.16.Simulation Results of the Designed PR Controller on Current-Tracking. (A) Measured Instantaneous Waveforms, And (B) Comparison of the Reference and Actual Output Grid-Tied Current.

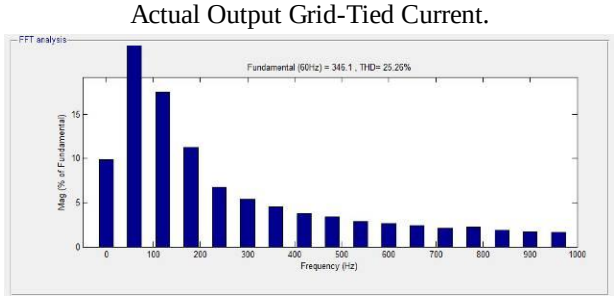

Fig.17.THD Performance of the MFGTI in different reference active power conditions..

B. Performance of the MFGTI on Power Quality Enhancement

In Fig. 2, just DG1 works as an MFGTI and the reference active/reactive power of DG1 and DG2 for power generation are 7kW/0Var and 8kW/0Var, respectively. The instantaneous current and power at PCC, as indicated in Fig. 2, are demonstrated in Fig. 19, when DG1 transfers from no compensation ($\alpha 1 = \alpha 2 = 0$) to full compensation ($\alpha 1 = \alpha 2 = 1$).

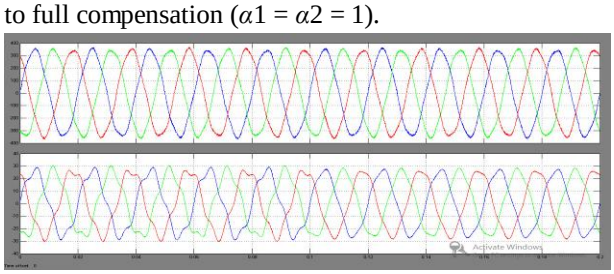

Fig.18. Three Phase Output Voltges(Vabc) And Currents(Iabc)

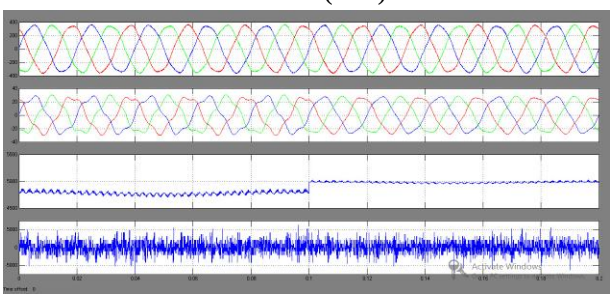

(a)

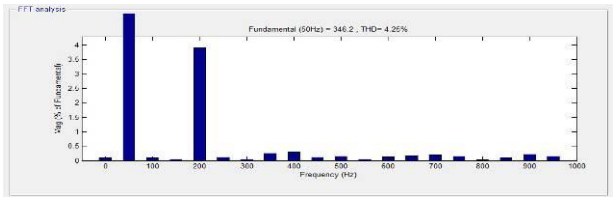

(b)

Fig .19.Simulation Results of The MFGTI From No Compensation ($A1 = A2 = 0$) To Full Compensation ($A1 = A2 = 1$). (A) The Waveforms at Pcc, (B) Harmonic Distribution of The Grid-Tied Current At Pcc.

C. Performance of the MFGTI on the Objective-Oriented Optimal Compensation

Firstly, take the case of objective I into consideration, to obtain the set CPQI after compensation and employ the minimum capacity of the MFGTI, using the mathematical model in Section III, flowchart in Fig. 7(a), and the simulation results in Fig. 19.

Objctive1*: Employing minimum capacity to maximally enhance the power quality of the micro-grid*

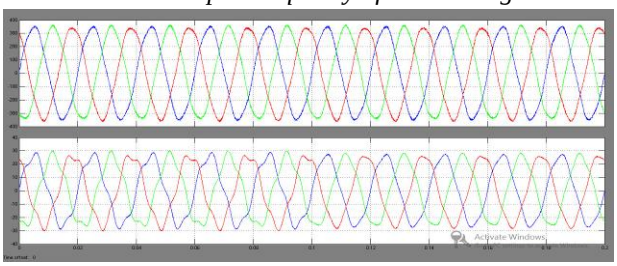

Fig.20. Three Phase Output Voltges(Vabc) And Currents(Iabc)

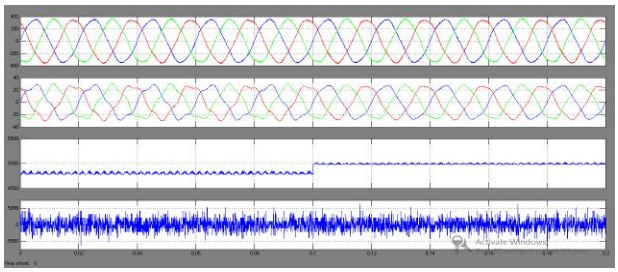

(a)

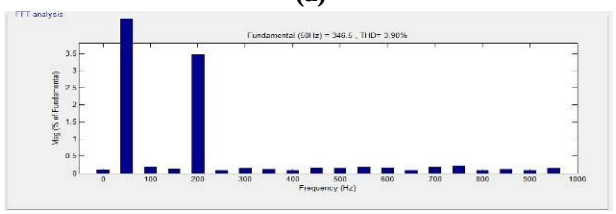

(b)

Fig.21. Simulation of dynamic responses of the MFGTI from no compensation to optimal compensation based on objective I ($\alpha 1 = 1$, $\alpha 2 = 0.8242$). (a) Waveforms of instantaneous current and power, (b) harmonic distribution of grid-tied current at PCC

Fig. 23 depicts the dynamic responses when DG1 transfers from no compensation model to objective II mode.But it is smaller than the one of objective I mode all the same, while the CPQI of objective II is larger than the one of objective I.

Objective ii: *Minimizing the CPQI in the condition of given capacity for power quality enhancement*

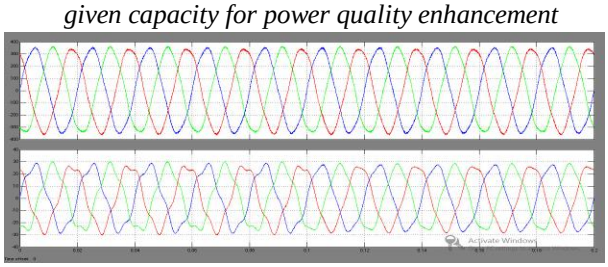

Fig.22. Three Phase Output Voltges(Vabc) And Currents(Iabc)

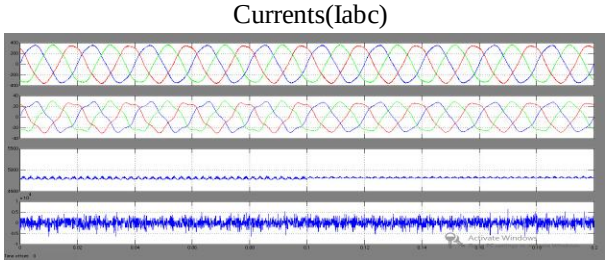

(a)

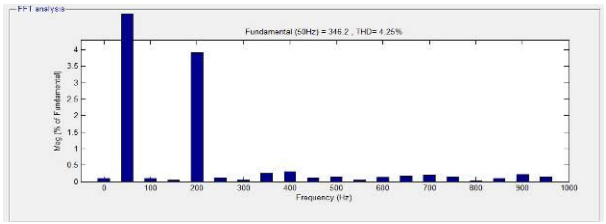

(b)

Fig.23. Simulation of dynamic responses of the MFGTI from no compensation to optimal compensation based on objective II ($\alpha 1 = 0.5106$, $\alpha 2 = 0.4327$). (a) Waveforms of the instantaneous current and power, (b) harmonic distribution of the grid-tied current.

VI.SIMULATION NALYSIS WITH PROPOSED SVPWM CONTROLLER

A. Performance of MFGTI on Power Generation with SVPWM

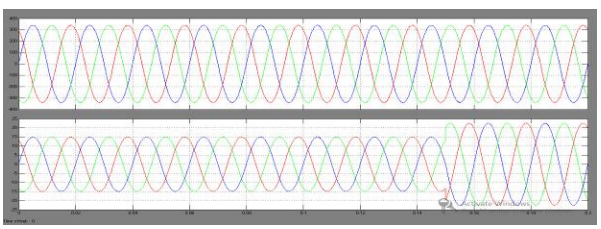

Fig.24. Three Phase Output Voltges(Vabc) And Currents(Iabc)

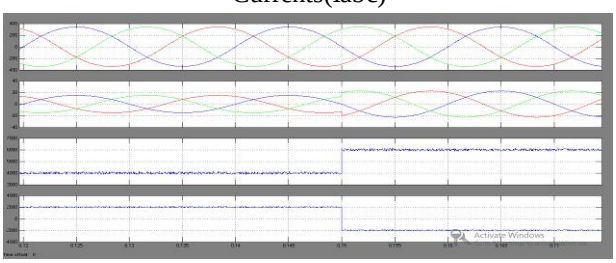

(a)

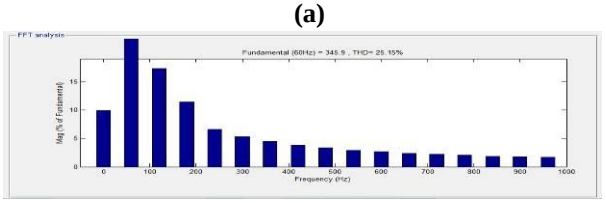

(b)

Fig.25.Simulation Results of the Designed PR Controller on Current-Tracking. (A) Measured Instantaneous Waveforms, And (B) Comparison of the Reference and Actual Output Grid-Tied Current.

B. Performance of the MFGTI on Power Quality Enhancement

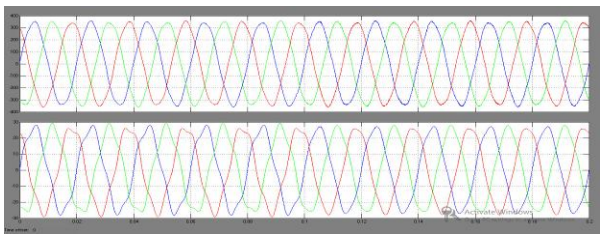

Fig..26. Three Phase Output Voltges(Vabc) And Currents(Iabc)

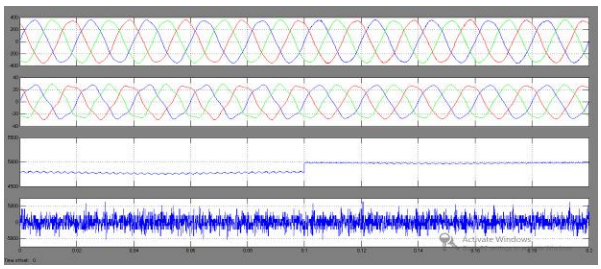

(a)

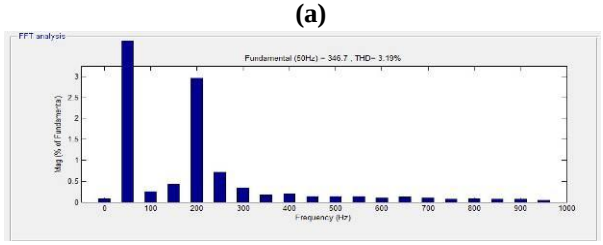

(b)

Fig .27.Simulation Results of The MFGTI from No Compensation ($A1 = A2 = 0$) To Full Compensation ($A1 = A2 = 1$). (A) The Waveforms at Pcc, (B) Harmonic Distribution of The Grid-Tied Current At Pcc

C. Performance of the MFGTI on the Objective-Oriented Optimal Compensation

objctive1*: Employing minimum capacity to maximally enhance the power quality of the micro-grid*

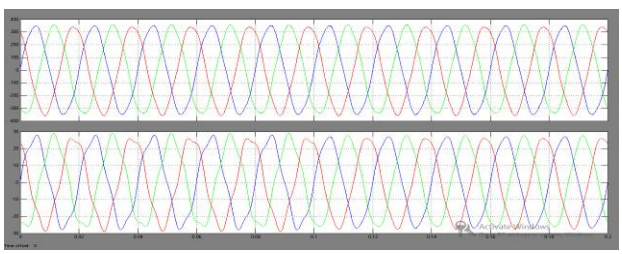

Fig.28. Three Phase Output Voltges(Vabc) And Currents(Iabc)

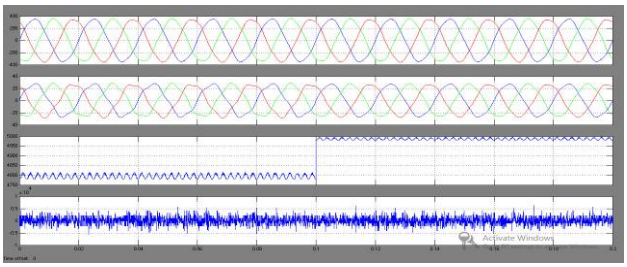

(a)

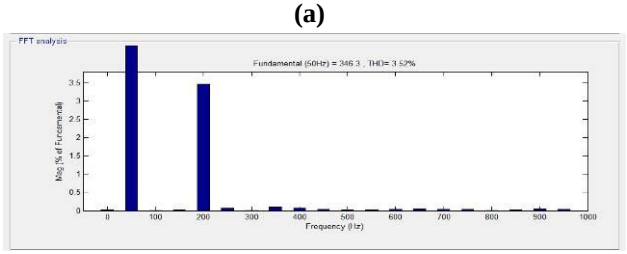

(b)

Fig.29. Simulation of dynamic responses of the MFGTI from no compensation to optimal compensation based on objective I ($\alpha 1 = 1$, $\alpha 2 = 0.8242$). (a) Waveforms of instantaneous current and power, (b) harmonic distribution of grid-tied current at PCC

Objective ii: *Minimizing the CPQI in the condition of given capacity for power quality enhancement*

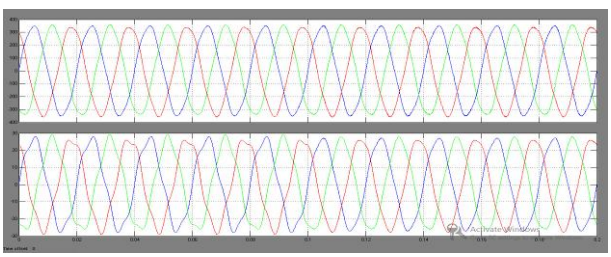

Fig.30. Three Phase Output Voltges(Vabc) And Currents(Iabc)

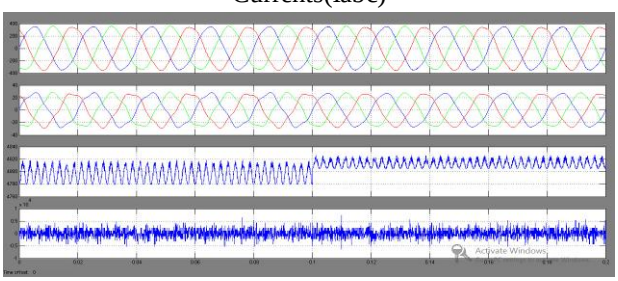

(a)

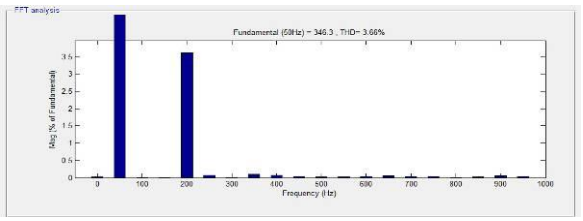

(b)

Fig.31. Simulation of dynamic responses of the MFGTI from no compensation to optimal compensation based on objective II ($\alpha 1 = 0.5106$, $\alpha 2 = 0.4327$). (a) Waveforms of the instantaneous current and power, (b) harmonic distribution of the grid-tied current

VII. CONCLUSIONS

To optimally handle the power quality issues in a micro-grid using an MFGTI with svpwm , an objective-oriented model is proposed in this paper based on AHP theory firstly. Then, the objectives to minimize the demanded capacity of the MFGTI (objective I) or minimize the CPQI (objective II) are presented.

Finally, the simulation results on a feeder of a micro-grid demonstration with two identical 10kVA DGs have verified the validations and feasibility of the proposed models and control strategies. Some conclusions can be drawn as follows.

1. The grid-tied inverter in the micro-grid has the auxiliary functionality to enhance the power quality of the micro-grid, but the functionality is limited by the available margin capacity of the MFGTI. Thus, how to optimally organize and control the MFGTI is a very urgent necessary. And the THD had reduced from 25.26% to 25.15%.

2. The proposed CPQI-based optimal model is simple and easy to carry out as an effective tool to quantify the power quality of the micro-grid. It also can guide the optimal power quality compensation and the on-grid electricity price of micro-grids in the power quality market in the near future. The THD value had reduced from 4.25% to 3.19% .

3. Two objective-oriented optimal compensation strategies are proposed in this paper. One can confirm the minimum compensation capacity of MFGTI in the

condition of the given CPQI; on the contrary, the other one can enhance the power quality of the micro-grid as good as possible in the condition of given available capacity of the MFGTI. The comparative performances and the best usage of the two proposed control strategies are also discussed. In objective 1 we have THD as 3.90% to 3.52% and in objective ii condition we have THD reduction from 4.25% to 3.66%.These two objectives can flexibly adapt the applications of the MFGTIs in the micro-grid and customize the power quality of the micro-grid.

REFERENCES

[1] P. C. Loh, D. Li, Y. K. Chai, and F. Blaabjerg, "Autonomous operation of hybrid microgrid with AC and DC subgrids," *IEEE Trans. on Power Electron.*, vol. 28, no. 5, pp. 2214-2223, May 2013.

[2] N. W. A. Lidula and A. D. Rajapakse, Microgrids research: A review of experimental microgrids and test systems," *Renew. Sust. Energy Rev.*, vol. 15, no. 1, pp. 186-202, Jan. 2011.

[3] Z. Zeng, R. Zhao, H. Yang, and S. Tang, "Policies and demonstrations of micro-grids in China: A review," *Renew. Sust. Energy Rev.*, vol. 29, pp. 701-718, Jan. 2014.

[4] H. Nikkhajoei and R. H. Lasseter, "Distributed generation interface to the CERTS microgrid," *IEEE Trans. on Power Del.*, vol. 24, no. 3, pp. 1598-1608, Jul. 2009.

[5] S. C. Tan, C. K. Lee and S. Y. Hui, "General steady-state analysis and control principle of electric springs with active and reactive power compensations," *IEEE Trans. on Power Electron.*, vol. 28, no. 8, pp. 3958-3969, Aug. 2013.

[6] J. He, Y. W. Li, F. Blaabjerg, and X. Wang, "Active harmonic filtering using current-controlled, grid-connected DG units with closed-loop power control," *IEEE Trans. on Power Electron.*, vol. 29, no. 2, pp. 642-653, Feb. 2014.

[7] J. H. R. Enslin and P. J. M. Heskes, "Harmonic interaction between a large number of distributed power inverters and the distribution network," *IEEE Trans. on Power Electron.*, vol. 19, no. 6, pp. 1586-1593, Nov. 2004.

[8] J. He, Y. W. Li, D. Bosnjak, and B. Harris, "Investigation and active damping of multiple resonances in a parallel-inverter-based microgrid," *IEEE Trans. on Power Electron.*, vol. 28, no.1, pp. 234-246, Jan. 2013.

[9] H. Xu, J. Hu and Y. He, "Operation of wind-turbine-driven DFIG systems under distorted grid voltage conditions: Analysis and experimental validations," *IEEE Trans. on Power Electron.*, vol. 27, no. 5, pp. 2354-2366, May 2012.

[10] J. Driesen, T. Green, T. Van Craenenbroeck, and R. Belmans, "The development of power quality markets," in *Proc. IEEE PES Winter Meeting*, 2002, pp. 262-267.

B. SIVA NAGA MALLESWARA RAO currently pursuing his M.Tech in electrical power systems in Prakasam engineering college, Kandukur, Andhra pradesh, affiliated to JNTU, Kakinada. He has done his B.Tech degree from A.B.R College of engineering & technology. Affiliated to JNTU, Kakinada, Andhra pradesh, India and his fields of interest include renewable energy sources, power systems and advanced controller.

V. HARI BABU presently working as Associate professor in prakasam engineering college, Kandukur, Andhra pradesh, India. Completed his M.Tech in Power Electronics from JNTU Kakinada. His fields of interest include Non Conventional Energy Sources, Advanced Control Techniques and Electrical Drives

M. BALA SUBBA REDDY currently is working as Associate Professor & H.O.D in electrical department of Prakasam engineering college, kandukur, Andhra pradesh, India. He had completed his Ph.D in power electronics from JNTU, Kakinada. His fields of interest include non conventional energy sources, electrical drives and power electronics